Stability Analysis of Prescribed Slip Surfaces Based on a Combination of the Equilibrium Equation and the Critical Unstable Condition

Lu Shi[1]; Bing Bai[2]; and Xiaochun Li[3]

Abstract: Stability analysis of potential slip surfaces is one of the core steps of slope safety evaluation. In this study, a novel model was developed that considers the critical unstable condition that represents the limit equilibrium and displacement constraints along a prescribed slip surface. The stress distribution and the safety factor of the prescribed slip surface in the critical state can be obtained by directly solving the nonlinear equations formed by the model. By incorporating the finite-element stress analysis, the proposed model does not require interslice force assumptions as do the traditional limit-equilibrium methods and can consider the influence of stress perturbation from outside of the slip body on its stability. The numerical algorithm is also detailed in the article. In addition, an analysis of three examples is carried out to validate the effectiveness of the proposed model and to demonstrate its feature of fast convergence. **DOI: 10.1061/(ASCE)GM.1943-5622.0001034.** © *2017 American Society of Civil Engineers.*

Author keywords: Slope stability; Factor of safety; Limit equilibrium method; Critical unstable point; Critical unstable condition; Strength-reduction method.

Introduction

Stability analysis is the precondition to designing a slope that should be stable and to taking reinforcement measures when the slope is suffering problems of instability.

There are many methods for evaluating slope stability, and the majority of them are limit-equilibrium methods (LEMs) [e.g., Bishop (1955); Morgenstern and Price (1965); Spencer (1967); Janbu (1975); Ahmed et al. (2012)] because of their relative simplicity and the experience accumulated by geotechnical practitioners for decades (Liu et al. 2012). In the LEM, a coefficient called factor of safety (FOS) is employed to reduce the shear strengths of all the points on the slip surface until the surface reaches the critical state or the so-called limit-equilibrium state. To solve the statically indeterminate problem, the slip body is discretized into many vertical slices with the introduction of interslice force assumptions, which are the main differences among the various LEMs. However, the assumption of the internal force may result in a notably different distribution of normal stress on the slip surface, thus affecting the calculated FOS. Furthermore, because the stress–strain behavior is

[1]Associate Professor, State Key Laboratory of Geomechanics and Geotechnical Engineering, Institute of Rock and Soil Mechanics, Chinese Academy of Sciences, Wuhan, Hubei 430071, China (corresponding author). ORCID: https://orcid.org/0000-0002-2040-5895. E-mail: shilu .whrsm@qq.com

[2]Associate Professor, State Key Laboratory of Geomechanics and Geotechnical Engineering, Institute of Rock and Soil Mechanics, Chinese Academy of Sciences, Wuhan, Hubei 430071, China. E-mail: bing_bai2@ 126.com

[3]Professor, State Key Laboratory of Geomechanics and Geotechnical Engineering, Institute of Rock and Soil Mechanics, Chinese Academy of Sciences, Wuhan, Hubei 430071, China. E-mail: xcli@whrsm.ac.cn

not covered in the LEM, the anchoring force is usually simplified as a concentrated force applied on one of the slices, and the influences of disturbances from outside the slip body, such as excavation and loading, cannot be considered.

As a result of the outstanding advantages of the finite-element method (FEM), FEM-based approaches have seen wide applications in slope engineering. Zienkiewicz et al. (1975) first proposed the idea of a shear strength-reduction method (SRM) based on the FEM, and later Donald and Giam (1992), Matsui and San (1992), Dawson et al. (1999), Griffiths and Lane (1999), Zheng et al. (2005), Bai et al. (2014), and Isakov and Moryachkov (2014), among others, adopted and developed it for slope stability analysis. The physical meanings of the FOS defined by the SRM and the LEM are actually the same. The difference is that the strength-reduction range in the SRM is the entire slope, whereas in the LEM, it is limited to a given slip surface. Many researchers [e.g., Cheng et al. (2007); Liu et al. (2015)] have compared the SRM with the LEM to illustrate their advantages and limitations. Generally speaking, the SRM is able to accommodate any slope shape, simulate various properties of the mechanical behavior, and bypass many of the deficiencies that are inherent within the LEM. More importantly, the SRM locates the critical slip surface automatically from the fields of displacement (Wang et al. 2016; Yuan et al. 2016), equivalent plastic strain (Zheng et al. 2009), or other parameters without the optimization measures. However, the SRM is unable to analyze a noncritical slip surface of interest (i.e., local minima), which may also need treatment in engineering practice, which is why Cheng et al. (2007) suggested that the LEM should be carried out as a cross reference.

Another FEM-based approach for calculating the FOS of a given slip surface is the enhanced limit-strength method (ELSM), in which the ratio of the shear strength integral to the shear stress integral along the slip surface is defined as the FOS (e.g., Brown and King 1966; Kulhawy 1969; Naylor 1982; Fredlund et al. 1999). The definition of the FOS by the ELSM for a circular slip surface is equivalent to that defined by the Fellenius method. The integral of the directional shear stress along a noncircular slip

surface has an uncertain physical meaning, although a number of examples have shown that the FOSs by the LEM and the ELSM are very close. Consequently, Ge (2010) proposed a modified ELSM called the vector-sum method, in which the principal sliding direction of the slip body is defined, and the stress on the slip surface is projected onto this direction for a vector integral. However, the concept of the principal sliding direction remains ambiguous, and there is no unified method to determine it. In addition, the stability analysis based on the stress field of the status quo in the ELSM does not obey Pan's extremum principle, as proven by Chen (1998).

To calculate the FOS of a prescribed slip surface based on the strength-reduction concept without any assumptions, a novel model that imposes additional constraints on the boundary-value problem of the equilibrium equation of the slope is proposed in this article. The constraints, including conditions of the stress and displacement on the slip surface, are used for describing the critical state of the slip surface. By incorporating the FEM, the FOS and the stress field in the critical state of the slip surface can be obtained by solving the nonlinear equations formed by the model with the Newton method. For comparison, the Morgenstern–Price (MP) method (Morgenstern and Price 1965) with an inter-slice function of a half sine and the SRM that performs the strength reduction only on the slip surface (termed SRM-slip) are considered.

Model for the Stability Analysis of a Given Slip Surface

Governing Equations of Stress Analysis Problem

Consider a two-dimensional (2D) slope Ω bounded by boundary Γ externally, in which the slip surface Γ_s separates the slope into a slip body Ω^+ and a slip bed Ω^-, as shown in Fig. 1. The *master–slave* concept in classic contact mechanics is adopted here, such that the master and slave bodies in this study pertain to each side of the slip surface Γ_s. Therefore, Ω^- is assigned to the master side, and Ω^+ is assigned to the slave side. For notational convenience, the superscripts $+$ and $-$ are used to denote the quantities associated with Ω^+ and Ω^-, respectively, and the subscript s is used to denote the quantities associated with Γ_s. Considering that the stability analysis is usually for Ω^+, Ω^- can be regarded as a rigid body. The boundary-value problems governing the equilibrium equation in this case can be written as

$$\nabla \cdot \sigma + b = 0 \quad in \ \Omega$$
$$\sigma \cdot n = \tilde{t} \ on \ \Gamma_t$$
$$u = \tilde{u} \ on \ \Gamma_u \tag{1}$$

where σ = Cauchy stress tensor; u = displacement vector; ∇ = gradient operator; b = body force vector; $\tilde{u}$ and $\tilde{t}$ = prescribed traction and displacement on the natural boundary Γ_t and the essential boundary Γ_u, respectively; $\Gamma_t \cup \Gamma_u = \Gamma$, $\Gamma_t \cap \Gamma_u = \varnothing$; and n = unit outward normal vector of Γ.

Considering a small deformation assumption, the geometric equation can be expressed as

$$\epsilon = \frac{1}{2}(\nabla u + u\nabla) \tag{2}$$
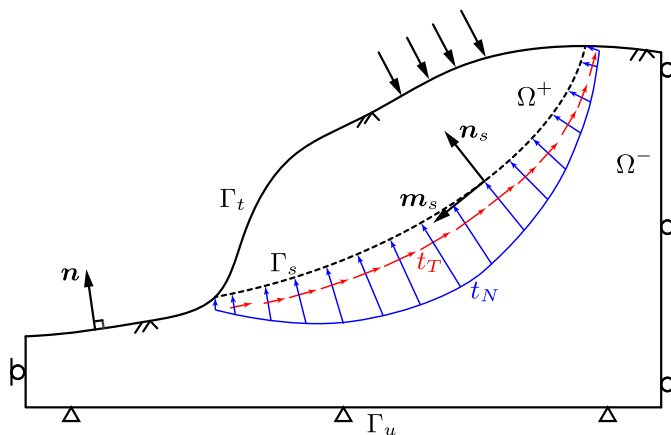
where ϵ = strain tensor.

Fig. 1. Definition of the 2D slope with a slip surface at the critical state

The relationship between the stress tensor σ and the strain tensor ϵ can be established through a constitutive equation, and the simplest one is linear elasticity, generally described as follows:

$$\sigma = \mathcal{D} : \epsilon \tag{3}$$

where $\mathcal{D}$ = fourth-order elastic tensor of the slope material with respect to a plane strain.

Because the slip surface is regarded as an interface to the slope, the boundary-value problems described previously can be augmented by

$$\sigma \cdot n_s = t \equiv -t_N n_s + t_T m_s \ on \ \Gamma_s \tag{4}$$

where n_s = unit outward normal vector to the slave side of the slip surface Γ_s; t is the traction acting on the slave side of the slip surface, which can be divided into the normal stress t_N (compressive stress is positive) and shear stress t_T; and m_s = unit tangential vector toward the sliding direction of the slip body. The traction acting on the Γ_s of the master body is $-t$, essentially the same as t but in the opposite direction.

Critical Unstable Condition

The limit equilibrium condition of any point x on the slip surface can be expressed as

$$t_T = \frac{1}{F_s}(t_N \tan\phi + c) \ \forall x \in \Gamma_s \tag{5}$$

where F_s = unknown FOS of the slip surface Γ_s; and ϕ and c = friction angle and cohesion of the slip surface, respectively. Thus, it can be seen that the limit-equilibrium condition contains the Mohr–Coulomb criterion and the shear strength reduction.

Substituting Eq. (5) into Eq. (4) yields

$$t = -t_N n_s + \frac{1}{F_s}(t_N \tan\phi + c)m_s \ on \ \Gamma_s \tag{6}$$

Clearly, the traction between the slip surface is related to only t_N and F_s.

For the contact problem, the two sides of the contact surface are initially in full contact, and the impenetrability conditions (also known as KKT conditions) are

$$g_N \leq 0, \ t_N \geq 0, \ g_N t_N = 0 \ \forall x \in \Gamma_s, \ \text{with} \ g_N = [\mathbf{u}] \cdot n_s \quad (7)$$

where $[\mathbf{u}] = \mathbf{u}^- - \mathbf{u}^+$ represents the relative displacement along the slip surface; and g_N is the relative normal displacement of the contact surface.

Eq. (7) implies that if $g_N < 0$, there is a gap between the two sides, and $t_N = 0$, and if $g_N = 0$ and $t_N \geq 0$, the two sides are in contact. For the contact condition of the slip surface Γ_s, the two sides always remain in contact, so the impenetrability condition can be simplified as

$$g_N = 0 \ \forall x \in \Gamma_s \quad (8)$$

In addition, because the slip surface is in the critical state, there should exist one point on the slip surface with the relative tangential displacement equaling zero, that is:

$$g_T = 0 \ \exists x \in \Gamma_s \ \text{with} \ g_T = -[\mathbf{u}] \cdot m_s \quad (9)$$

The physical meaning of Eq. (9) is that when the slip surface is in the critical state, there should be one last point on the slip surface that is about to slide ($g_T = 0$) when the shear stress reaches the shear strength. At that time, the relative shear displacements of the other points on the slip surface are larger than zero. This point is called the critical unstable point (CUP). The influence of the CUP selection on the FOS will be discussed in detail.

The combination of Eqs. (6), (8), and (9) is called the critical unstable condition throughout the paper, and it reflects the stress and the displacement constraints of the slip surface in the critical state.

FEM-Based Numerical Model

Treating the slip surface as the external boundaries for Ω^+ and Ω^-, according to the principle of virtual work, the equivalent weak form of the previously mentioned boundary-value problem with the traction between the slip surface can be expressed as

$$
\begin{aligned}
\delta \Pi &= \delta \Pi_u - \int_{\Gamma_s} [\delta u] t d\Gamma \\
&= \delta \Pi_u + \int_{\Gamma_s} \left[\delta g_N t_N + \delta g_T \frac{1}{F_s} (t_N \tan \phi + c) \right] d\Gamma = 0
\end{aligned}
\quad (10)
$$

with

$$\delta \Pi_u = \int_\Omega \delta \varepsilon : \mathcal{D} : \epsilon d\Omega - \int_\Omega \delta u \cdot b d\Omega - \int_{\Gamma_t} \delta u \cdot \tilde{t} d\Gamma \quad (11)$$

where δ = virtual; and Π_u = total potential energy for the original problem without the traction on the slip surface.

The normal stiffness k_N, which is equivalent to the penalty parameter in the penalty function method that imposes the constraint of Eq. (8), is introduced in this study. Consequently, we have

$$t_N = k_N g_N \ \forall x \in \Gamma_S, \quad (12)$$

in which $k_N \gg 1$. Compared to the Lagrange multipliers method, the penalty method has the advantage of introducing no new degree of freedom and zero diagonal terms. However, the normal stiffness allows the two sides of the slip surface to penetrate into each other slightly, that is, $g_N > 0$, which is approximately satisfied by Eq. (8).

To avoid the influence of the normal stiffness selection on the normal stress distribution along the slip surface, the augmented Lagrange multipliers method (see Simo and Laursen 1992; Hirmand et al. 2015) is implemented for dealing with the constraint of Eq. (8):

$$t_N = \lambda_N + k_N g_N \ \forall x \in \Gamma_S, \quad (13)$$

where λ_N, the augmented Lagrange rebounding force, is not an unknown as in the Lagrange multiplier method and can obtained by augmentation iterations. The determination of λ_N in the mth step can be updated with

$$\lambda_N^{(m+1)} = \lambda_N^{(m)} + k_N g_N^{(m)} \ \text{with} \ \lambda_N^{(0)} = 0 \quad (14)$$

Substituting Eq. (12) into Eq. (10), the variational formulation in each augmentation can be written as

$$
\begin{aligned}
F_s \delta \Pi_u &+ \int_{\Gamma_s} (F_s \delta g_N + \delta g_S \tan \phi) k_N g_N d\Gamma + \int_{\Gamma_S} \\
&\times (F_s \delta g_N + \delta g_S \tan \phi) \lambda_N^{(m)} d\Gamma + \int_{\Gamma_S} c \delta g_S d\Gamma = 0
\end{aligned}
\quad (15)
$$

According to the finite-element interpolation, the displacement and strain fields can be described, respectively, as

$$u(x) = \sum_{I \in \mathcal{N}} N_I \overline{u}_I \equiv N(x) \overline{u} \quad (16)$$

$$\epsilon(x) = \sum_{I \in \mathcal{N}} B_I \overline{u}_I \equiv B(x) \overline{u} \quad (17)$$

where $\mathcal{N}$ = node set of the finite-element mesh; N_I = shape function; and $\overline{u}_I$ = vector of nodal degrees of freedom; in addition, B is the strain matrix that can be obtained using $B = \mathcal{S} N$, in which $\mathcal{S}$ is a suitable linear differential operator and can be determined by Eq. (2).

By approximating the virtual displacement and strain fields $\delta u(x)$ and $\delta \epsilon(x)$ in analogy with Eqs. (15) and (16), the discrete form of the variational formulation can be derived as

$$(F_s K + F_s K_{SN} + K_{ST}) \overline{U} + F_s Q_{SN}^{(m)} + Q_{ST}^{(m)} - F_s Q = 0 \quad (18)$$

with

$$K = \int_\Omega B^T D B d\Omega$$

$$K_{SN} = k_N \int_{\Gamma_s} N^T n_S n_S^T N d\Gamma$$

$$K_{ST} = k_N \int_{\Gamma_s} \tan \phi N^T m_S n_S^T N d\Gamma$$

$$Q_{SN}^{(m)} = \int_{\Gamma_s} \lambda_N^{(m)} N^T n_S d\Gamma$$

$$Q_{ST}^{(m)} = \int_{\Gamma_s} \tan \phi \lambda_N^{(m)} N^T m_S d\Gamma + \int_{\Gamma_s} c N^T m_S d\Gamma$$

$$Q = \int_\Omega N^T b d\Omega + \int_{\Gamma_t} N^T \tilde{t} d\Gamma$$

where $\overline{U}$ = displacement vector of all the mesh nodes; D = elastic matrix; and $Q_{SN}^{(m)}$ and $Q_{ST}^{(m)}$ = nodal forces that are induced by augmentation traction components perpendicular to and parallel to the

slip surface, respectively, and can be calculated with the known nodal value of $\overline{\lambda}_N^{(m)}$ on the slip surface at the mth augmentation iteration.

Selecting one of the nodes χ on the slip surface as the CUP, the constraint condition of Eq. (9) can be written as

$$K_{\text{cup}}\overline{U} = 0 \quad \text{with} \quad K_{\text{cup}} = k_N m_S^{\text{T}}(\chi)N(\chi) \tag{19}$$

in which k_N is used to make the nonzero elements in matrix K_{SN} and vector K_{cup} have the same order of magnitude.

A stability analysis of the slip surface based on Eqs. (17) and (19) involves solving the following nonlinear equations with the unknowns of $\overline{U}$ and F_s:

$$H^{(m)}\left(\overline{U}; F_s\right) = \begin{bmatrix} (F_s K + F_s K_{SN} + K_{ST})\overline{U} + F_s Q_{SN}^{(m)} + Q_{ST}^{(m)} - F_s Q \\ K_{\text{cup}}\overline{U} \end{bmatrix}$$

$$= 0 \tag{20}$$

To summarize, some advantages of the proposed model for solving the FOS are as follows: (1) The interslice force assumption is no longer required as in the traditional LEMs; (2) by employing the finite-element stress analysis, the consideration of reinforcements and disturbances from outside of the slip body is more reasonable; (3) the FOS of the slip surface can be obtained by solving the nonlinear equations directly, and some solution techniques such as the Newton method that are significantly faster than the bisection search used in the SRM can be applied.

Solution Algorithm

The Newton method (see Burden and Faires 2011) is used to solve the nonlinear equations of Eq. (20). In the ith step of the Newton iteration, the Jacobian matrix is

$$J(X^{i-1}) = \begin{bmatrix} F_s^{i-1}(K + K_{SN}) + K_{ST} & (K + K_{cn})\overline{U}^{i-1} + Q_{SN}^{(m)} - Q \\ K_{\text{cup}} & 0 \end{bmatrix} \tag{21}$$

where $X^{\text{T}} = \begin{bmatrix} \overline{U}^{\text{T}} & F_s \end{bmatrix}$.

The new values of the unknowns at this step can be updated with

$$X^i = X^{i-1} - J^{-1}(X^{i-1}) \cdot H(X^{i-1}) \tag{22}$$

In solving the equations, the processes of the Newton iteration and the augmentation loop end when the following conditions are satisfied, respectively:

$$\eta_g = |H|/|Q| < e_g \tag{23}$$

$$\eta_l = \ell^{-2}\int_{\Gamma_S} g_N d\Gamma < e_l \tag{24}$$

where ℓ = length of the slip surface, that is, $\ell = \int_{\Gamma_S} d\Gamma$. In the subsequent examples, e_g and e_l in this study are set to 10^{-6} and 10^{-10}, respectively.

Based on the proceeding derivations and the solution method, a code named FELE^{2D} is developed. The details of the algorithm are shown in Fig. 2.
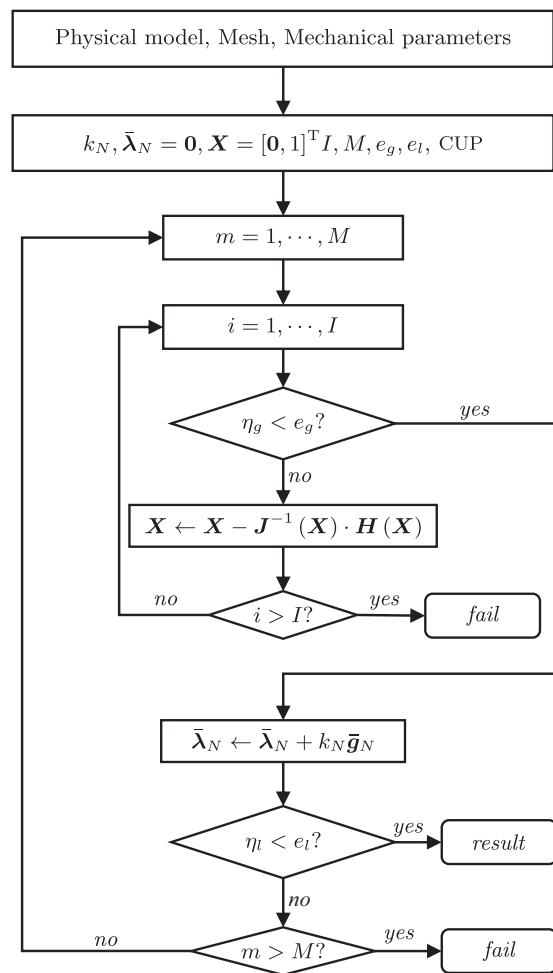

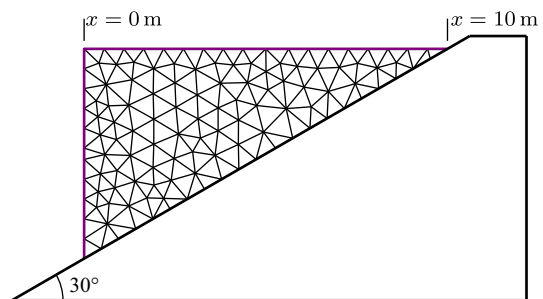**Fig. 2.** Flow diagram of algorithm of FELE^{2D}

Fig. 3. Example 1: A 2D wedge on a planar slope; the wedge is discretized into 192 triangular elements with 122 nodes, and the slip bed is treated as a rigid body

Examples and Verifications

Example 1: Planar Slip Surface

Fig. 3 shows a straightforward example of a planar slip surface. The rock-like material has an elastic modulus E of 28 GPa, Poisson's ratio ν of 0.23, and unit weight γ of 27 kN·m^3. The planar slip surface has an incline angle θ of 30° and length of 11.55 m. The volume V of the slip body is 28.87 m^3/m. The analytical expression of the FOS for the slip surface is given by

© ASCE

04017118-4

Int. J. Geomech.

$$F_s = \tan\phi \cot\theta + \frac{\ell c}{V \gamma \sin\theta} \qquad (25)$$

Table 1 lists the FOSs calculated by the analytical expression and the proposed method with k_N equaling 100 GPa/m. The FOSs of the four cases acquired using the proposed method were found to be very consistent with those by the analytical solution, which indicates that the accuracy of FELE^{2D} is very high. The convergence information in solving Case 4 plotted in Fig. 4 exhibits a rate of quadratic convergence of the Newton iteration, such that the convergence is achieved in no more than three iterations in each augmentation. Note that the Newton algorithm converges in only one iteration within the subsequent augmentations because the FOS and the field of displacement from the first augmentation are quite close to the final solution. In addition, the impenetrability condition could be satisfied at a desired level of accuracy by three augmentations. However, the convergence rate of the augmented Lagrange multipliers method is influenced by the normal stiffness (Hirmand et al. 2015). Technically, by setting k_N three orders of magnitude larger than the maximal diagonal element in K, it is possible to guarantee a fast convergence rate and avoid an ill-conditioned penalty formulation.

The FOSs of the wedge in Case 4 calculated using the MP, the SRM-slip, and the proposed method were 1.593, 1.607 and 1.593, respectively, thus differing very little. In this analysis by the MP, the slip surface was divided equidistantly into a total of 25 slices along the x-axis. In this analysis by the SRM-slip, the penalty method with both the normal and tangential penalty numbers equaling 100 GPa was adopted to enforce the normal and tangential constraints.

In Fig. 5, a comparison of the normal stresses along the planar surface calculated by these three methods in Case 4 is presented. The curve of the normal stress distribution from the MP shows a linearly decreasing trend from left to right with a slight sinusoidal variation because the MP regards the slip body as a rigid body and assumes that the normal and tangential forces between the slices have a relation of half sine function. On the contrary, the proposed method and the SRM-slip are both based on the FEM, and the slip body is regarded as a deformable body. Therefore, the distributions of normal stress acquired are very consistent and different from those obtained by the MP. However, after 16 iterations of the bisection search, the FOS obtained from the SRM-slip was 1.607, which is slightly larger than the analytical value, indicating that the SRM-slip might be susceptible to the unstable criterion. Moreover, it has a lower computational efficiency than the proposed method from the perspective of the number of iterations. Although the augmentation can greatly reduce the penetration of the two sides of the slip surface, it had almost no impact on the FOS and the normal stress distribution of the planar slip surface, as shown in Figs. 4 and 5.

If the finite-element model for a slip body is established upon the coordinate system with the x-axis parallel to the planar slip surface, the constraint on the tangential displacement of a point on the slip surface is equivalent to eliminating the rigid-body motion in the x-direction in the case of all the external forces, including gravity and the normal and shear stresses on the slip surface, satisfying the force and moment balances. In other words, the selection of the CUP will cause rigid-body motion only along the slip surface without changing the stress field of the slip body, which can be proven by a translational relationship between the curves of the tangential displacement distribution corresponding to three different CUPs, as shown in Fig. 6. Therefore, the selection of the CUP for the planar slip surface has

Table 1. FOSs Obtained Using the Analytical Method and the Proposed Method for Example 1 with Four Groups of Parameters

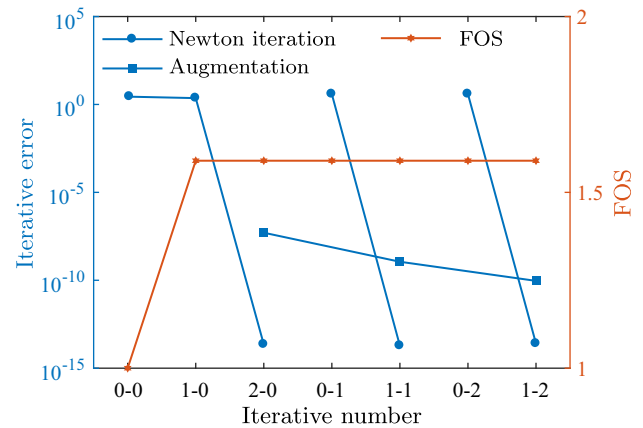|	Shear strength parameters		FOS	
Case	c (kPa)	ϕ (°)	Analytical solution	FELE^{2D}
1	0	35	1.21280	1.21280
2	0	30	1.00000	1.00000
3	0	25	0.80767	0.80767
4	20	30	1.59259	1.59259

Fig. 4. Convergence profiles in solving Case 4 of Example 1 by the FELE^{2D}; the indices of the x-axis with a format of i-m denotes the ith Newton iteration in the mth augmentation
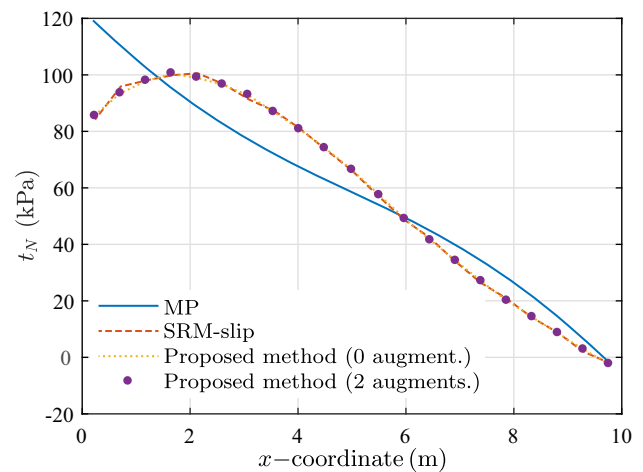

Fig. 5. The distributions of normal stress on the planar slip surface in Example 1 using the MP and the proposed method with and without augmentation (Case 4)

no effect on the FOS and the stress distribution. However, according to the definition of the CUP, the true CUP for Example 1 is the rightmost point on the slip surface whose tangential displacement is the smallest among all the points on the slip surface and equals zero. The displacement field of the slip body with the actual CUP is shown in Fig. 7. Apparently, it can tell the situation of the displacement that already happened in different parts of the slip body before it loses its stability.

Example 2: Circular Slip Surface

An example slope from test problem EX1(d) of the Association for Computer Aided Design, Australia (ACADS) (Donald and Giam 1992) will be analyzed to illustrate the proposed procedure for a circular slip surface. The geometry of the slope is plotted in Fig. 8. The impact of groundwater is not considered, and the soil parameters are listed in Table 2. The analyzed circular slip surface, which passes through Points A and C with a radius of 19.616 m, is the critical slip surface of the slope searched by *SLIDE* with the Bishop simplified method (Bishop 1955) very close to the critical slip surface from Chen (2003) using the STAB code. In addition, the seismic force is presumed to be a pseudostatic force that acts in the horizontal direction with a seismic coefficient of 0.15. As in Example 1, the slip bed is still regarded as a rigid body, so only the slip body is discretized. In this part, two cases were studied: Case 1 had the same conditions as the original test problem without reinforcement, and Case 2 was a multilayered sliding body with a support (Fig. 8).

Based on the Bishop simplified method, Donald and Giam (1992) recommended the overall FOS of the slope to be 1.0. In this analysis for Case 1, the FOSs of the slip body determined by the MP and the proposed method ($k_N = 10^6$ kPa/m) were 0.987 and 0.993, respectively, which are very close to the previous results. However, there is a difference between the corresponding normal stress distributions shown in Fig. 9, which means that the FOS of the circular slip surface is insensitive to the normal stress distribution, even though the slope is inhomogeneous. As shown in Fig. 10, the Newton method also exhibited good convergence for a circular slip surface. Moreover, the augmentation still had a negligible influence on the FOS of a circular slip surface, as shown by a comparison of
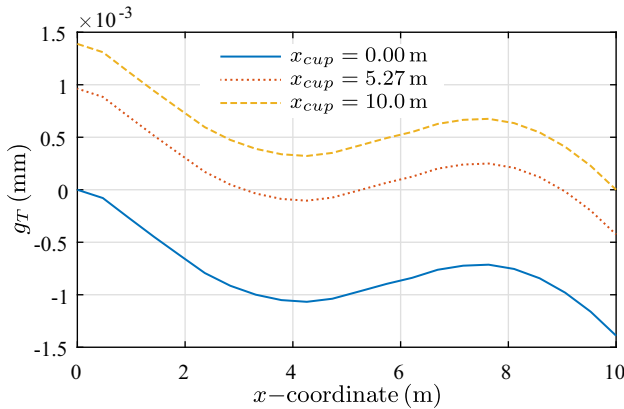

Fig. 6. Distributions of relative tangential displacement on the planar slip surface in Example 1 with different CUPs (Case 4)
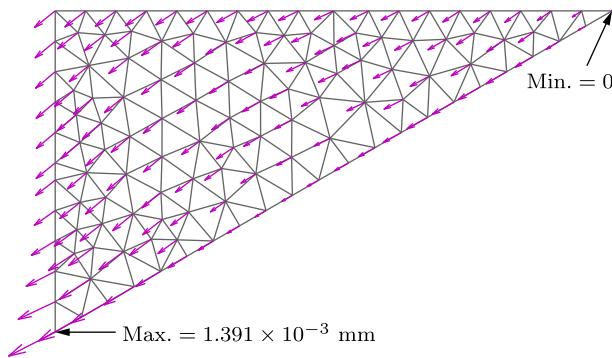

Fig. 7. Total displacement contour of the wedge in Example 1 with the *x*-coordinate of the CUP equaling 10 m (Case 4)

Table 2. Physical and Mechanical Properties of the Three Soil Layers in Example 2

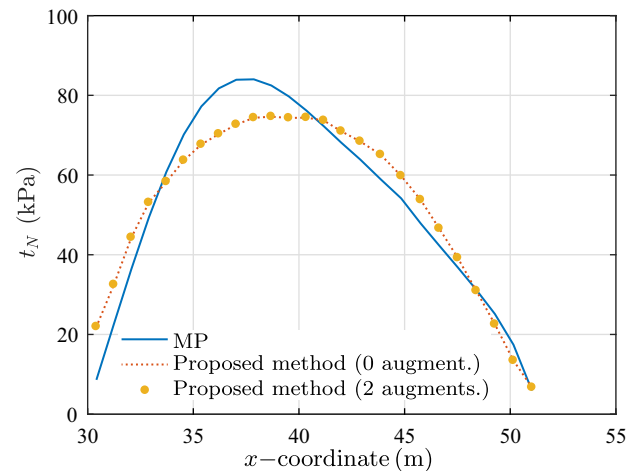| Layer	c (kPa)	ϕ (°)	γ (kN·m^3)	E (kPa)	ν
1	0.0	38.0	19.5	1.0×10^4	0.25
2	5.3	23.0	19.5	1.0×10^4	0.25
3	7.2	20.0	19.5	1.0×10^4	0.25

Fig. 9. Distributions of normal stress on the slip surface from the MP and the proposed method with and without augmentation for Case 1 of Example 2
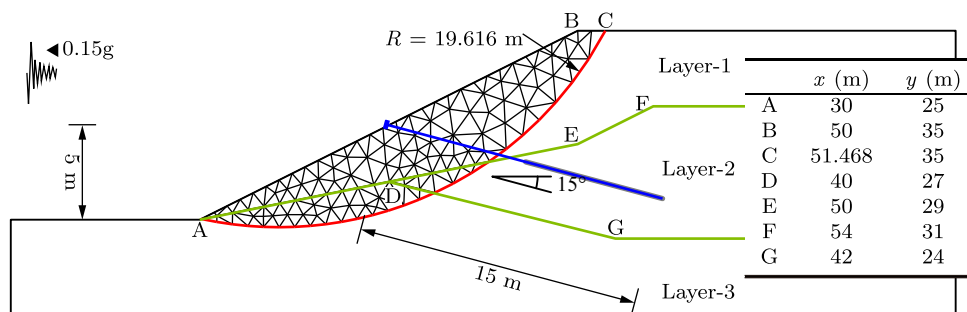

Fig. 8. Example 2: A multilayered soil slope with a circular slip surface; the slip body is discretized into 200 triangular elements with 129 nodes
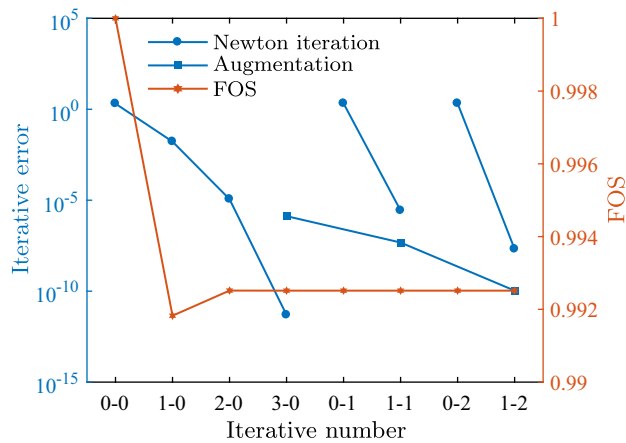
Fig. 10. Convergence profiles in solving Case 1 of Example 2 by the FELE^{2D}
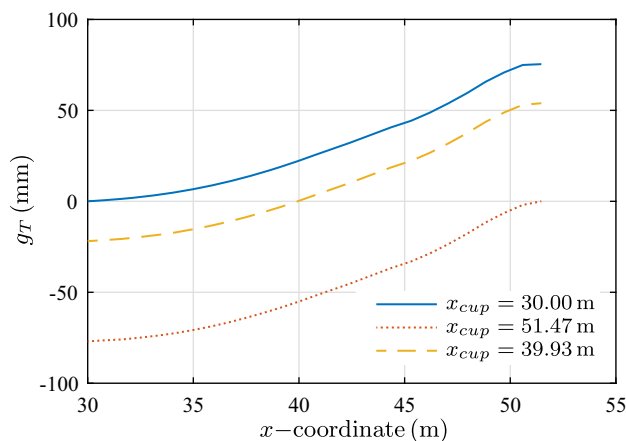

Fig. 11. Distributions of relative tangential displacement on the slip surface in Example 2 corresponding to different CUPs (Case 1)

the normal stress distributions from the proposed method with and without augmentation (Fig. 9).

Similarly, the role of the CUP in the circular slip surface is to eliminate the rigid-body rotation around the center of the circular slip surface, which can be further testified by the distribution of the relative tangential displacement shown in Fig. 11. Thus, selecting a random point as the CUP for a circular slip surface will not affect the final results except for the displacement field.

For Case 2, a row of grouted tiebacks was added to the slope at an angle of –15° from the horizontal. The tieback was 15 m long, and the spacing between each tieback was 2.5 m. Each tieback was pretensioned with a 100-kN active force on the anchor point. Typically, the forces exerted by a resistant element always act on the point of intersection of the slip surface and the resistant element in the LEM. Therefore, the normal stress of the slice upon which the support force is applied is significantly higher than that of the surrounding slices, as is illustrated in Fig. 12. In contrast, the proposed method regards the support as a concentrated load on the anchor point, which is more consistent with the reality. As a result, the normal stress of the part near the tieback is increased to a certain extent. Because the friction angle of Soil Layer 1 was clearly higher than that of the other two layers, and the slice on which the support force was exerted was situated in only this layer, the calculated reinforcement effect from the perspective of the FOS by the MP (from 0.987
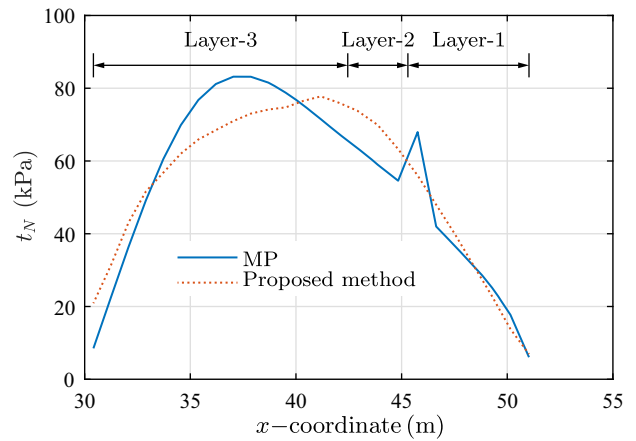

Fig. 12. Distributions of normal stress on the slip surface using the MP and the proposed method (Case 2 of Example 2)

to 1.051) is surely superior to that by the FELE^{2D} (from 0.993 to 1.045). Note that if the support element is considered to interact with the discretized slope bed by the proposed method, the stress distribution will be closer to the reality.

Example 3: Polyline Slip Surface

The example of a polyline slip surface is taken from test problem EX3(b) of ACADS (Donald and Giam 1992), as shown in Fig. 13. In the slope, there is a 0.5-m-thick weak interlayer, whose boundary is not considered to improve the mesh quality. However, the shear strength parameters of the slip surface within the interlayer were set to the actual values. Donald and Giam (1992) specified the slip surface AEFD, of which the segment EF in the weak interlayer will be studied here. The phreatic line is assumed to be at the bottom of the interlayer, and the geotechnical parameters of the soil layers are given in Table 3. k_N was set to 10^7 kPa/m. Two cases were studied for this example: Case 1 had same conditions as the original test problem, and Case 2 was tunneling beneath the slip surface.

Unlike the previously mentioned examples of planar and circular slip surfaces, the FOS of the polyline slip surface varies for different CUPs, as presented in Fig. 14. Therefore, how to choose the actual CUP is the problem to be settled first in the proposed model. According to Pan's extremum principle, for a given slip surface, the normal stress on the slip surface can be self-adjusted to maximize the slip resistance (Chen 1998); therefore, the CUP should be selected at the rightmost side of the slip surface, where the FOS of the slip surface can reach the maximum (i.e., 1.458). Fig. 14 also presents the distributions of g_T on the slip surface corresponding to two different candidate CUPs. By comparing the curves of the g_T distribution and the FOS variation, it is observed that the FOS corresponding to a candidate CUP is negatively correlated with the relative level of the g_T on this point. Therefore, the previously determined CUP is the point with the minimal g_T, which is in line with the definition of the CUP. Moreover, adjusting the normal stress on the slip surface to maximize its antisliding performance requires the occurrence of a relative tangential displacement along the slip surface, which should point to the sliding direction. Therefore, the actual CUP can also be automatically determined to be the node with the minimal g_T by a trial calculation, in which the CUP is selected arbitrarily on the slip surface. In this example, the leftmost Point A on the slip surface is first selected as the CUP, and then the uppermost Point D with the smallest g_T is selected as the actual CUP. With D as the CUP, the g_T of all the points on the slip surface except the CUP itself is positive. The convergence
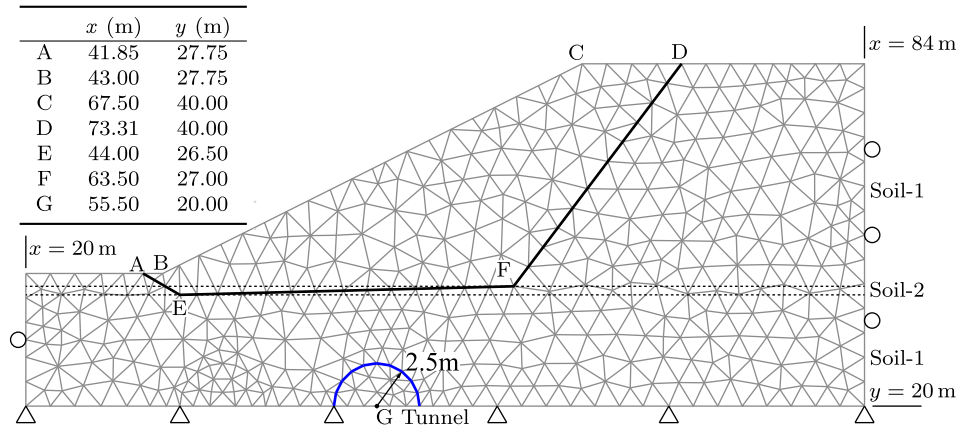
	x (m)	y (m)
A	41.85	27.75
B	43.00	27.75
C	67.50	40.00
D	73.31	40.00
E	44.00	26.50
F	63.50	27.00
G	55.50	20.00

Fig. 13. Example 3: A slope with a polyline slip surface; the model mesh has 472 nodes and 786 triangular elements

Table 3. Physical and Mechanical Properties of the Two Soil Layers in Example 3

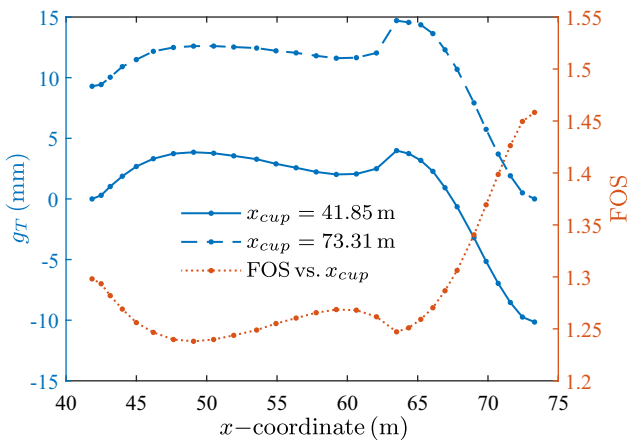| Soil	c (kPa)	ϕ (°)	γ (kN/m^3)	E (kPa)	ν
1	28.5	20.0	18.84	6.0×10^4	0.25
2	0.0	10.0	18.84	—	—

Fig. 14. The FOS for Case 1 of Example 3 varies with the position of the CUP; the distributions of the relative tangential displacement along the slip surface with two different CUPs are plotted for comparison

Fig. 15. Convergence profiles for Case 1 of Example 3 using the FELE^{2D} with the x-coordinate of the DCP equaling 73.31 m

Fig. 16. Comparison of normal stress distributions from the MP and the proposed method for Case 1 of Example 3; the normal stress distributions before and after tunneling by the proposed method are also compared

rate of the proposed method is also very fast for the polyline slip surface, as shown in Fig. 15.

The final FOS of Case 1 from the proposed method was 1.458, which is higher than the 1.266 obtained by the MP method by approximately 13%. For this example, there was also a relatively large difference in the FOSs within the LEMs, and the minimal and maximal values among the results collected by Donald and Giam (1992) were 1.195 and 1.450, respectively. It is hard to determine which is more accurate, but the LEM clearly does not take into account that the slip body needs to be deformed after a slight slip along the polyline slip surface. Excluding the effect of abrupt changes in the direction of the polyline slip surface, the distribution of the normal stress determined by the MP shown in Fig. 16 was actually very smooth. By contrast, the normal stress curve obtained by the proposed method had a significant jump at the endpoints E and F. If a candidate CUP (e.g., Point A) makes the g_T at the
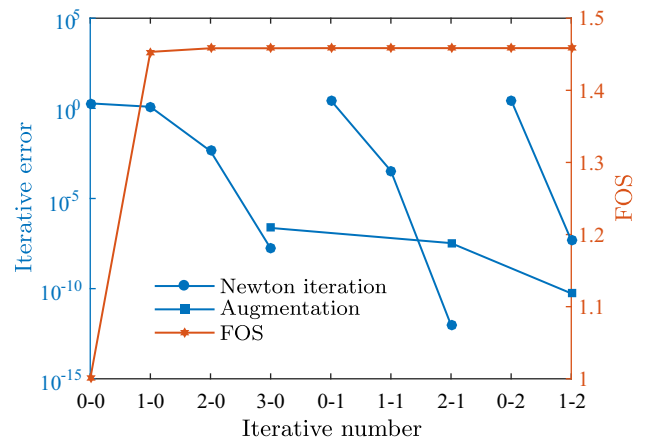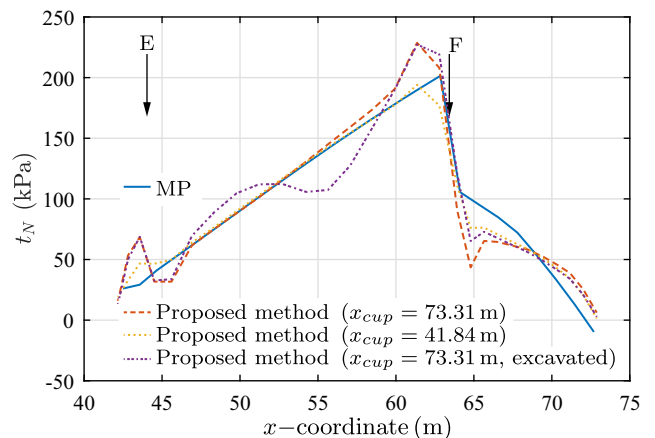
endpoint smaller, the corresponding results will be closer to the results by the MP.

For Case 2, a tunnel with a diameter of 5 m was arranged under the slip surface. The center of the tunnel was located at Point G, as

shown in Fig. 13. Although the excavation of the tunnel did not alter the geometry of the slip body, it could affect the FOS of the slip surface because of the disturbance to the stress field within the slope. For simplicity, the soil body was assumed to be elastic, with no tunnel support. Fig. 16 shows the changes in the normal stress distribution along the slip surface before and after tunneling. Because the MP is a rigid LEM and is incapable of handling the disturbance caused by tunneling beneath the slip surface, the normal stress distribution acquired from the MP will not change. After excavation, the normal stress of the region above the tunnel was reduced, leading to a redistribution of the normal stress on the entire slip surface. Therefore, the FOS of the slip surface after tunneling predicted by the proposed method decreased from 1.458 to 1.361. It should be acknowledged that the perturbation of the stress field was not as pronounced as described previously because of the presence of the tunnel support in reality. However, as an illustrative case, the authors want to emphasize that the effects of the stress perturbation can be considered by the proposed method. Positively, a more rational consideration of the realities needs further development of the FELE^{2D}, including the implementation of elastoplastic models, support elements, and groundwater.

Discussion of the Examples

These examples have shown the effectiveness and advantages of the proposed method. Because there is a new concept of CUP and a few techniques are involved in this method, there might be some potential issues to be improved, as follows:

1. The augmented Lagrange multipliers can eliminate the drawbacks of the penalty and Lagrange multipliers techniques and achieve a predetermined tolerance for the impenetrability condition of the slip surface. Nevertheless, its iterative procedure requires additional computation, which is detrimental to the optimization analysis for locating the critical failure surface. Conversely, the FOS can converge in the initial augmented Lagrange step. Therefore, taking the FOS tolerance (e.g., 0.001) as the convergence index, the convergence of the double loop algorithm in the solution procedure of the augmented Lagrange multipliers method can be accelerated. Furthermore, now that the augmentation has a negligible influence on the FOS and the normal stress distribution of the circular slip surface for the previous three examples, enabling the second augmentation is not necessary.

2. The CUP, which establishes the critical state for a slip surface along with the limit-equilibrium condition, is the core of the proposed method. Mathematically, it introduces an additional equation, and the FOS as an unknown can be solved together with the displacement field from the equations. Interestingly, the determination of the CUP complies with both its physical meaning and Pan's extremum principle. However, the authors cannot give the reason why the FOS can be maximized with the point of minimal g_T on the slip surface as the CUP.

   In addition, a trial procedure is required to locate the actual CUP. By examining the distribution of the failure approaching index (FAI, i.e., the ratio of shear strength to shear stress) on the slip surface, a potential answer can be found to minimize the computation caused by the trial. The CUP of each example corresponds to the location where the FAI is the maximum, as shown in Fig. 17. That is, the CUP is usually the point that is the least likely to fail on the slip surface. Note that the FAI at the rightmost point in Example 3 is actually infinite because its shear stress is negative. Alternatively, the CUP can be determined by finding the position with the maximal FAI, which can reduce the number of nonlinear equations that must be solved. Moreover, carrying out the calculation of the FAI can provide
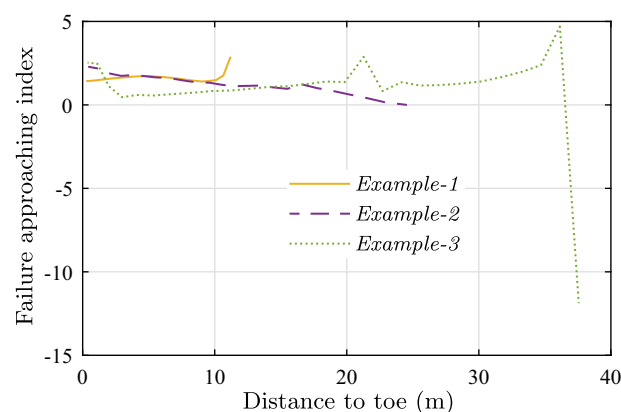

Fig. 17. Distribution of FAI on the slip surfaces of Example 1 (Case 4), Example 2 (Case 1), and Example 3 (Case 1); the *x*-axis is the distance from the toe along the slip surface

an initial value for the Newton iteration so that the convergence can be accelerated.

3. Similar to the LEM, the proposed method is used for the analysis of a given slip surface of a slope, so an optimization technique is needed to locate the critical slip surface. For cases such as Example 2, if considering only the mesh of the slip body, the calculation quantity of the proposed method should be similar to that of the LEM. However, if considering the entire slope, mesh reconstruction will be performed for every analyzed slip surface, which increases the difficulty of identifying the critical slip surface. Therefore, the extended FEM developed by Belytschko and Black (1999) can be adopted, and the slip surface can be regarded as a crack throughout the slope to avoid mesh reconstruction. Technically, each node can be preset with two enriched freedoms, and each element can be preset with a certain number of integral points, all of which can be activated if needed, thus greatly improving the search efficiency.

4. Solving the FOS of a slip surface is a statically indeterminate problem. Additional constraint conditions must be introduced to make the problem determinate in various methods. In other words, the constraint conditions a method adopts, to some extent, limit the application scope of the method. Cheng et al. (2008) found that the influence of the interslice force function on the FOS of a prescribed slip surface cannot be ignored in some circumstances and suggested taking the maxima as the FOS, which is consistent with Pan's maximum principle. Instead of the interslice force assumption, the proposed method employs the compatibility condition of deformation and the critical unstable condition to make the problem determinate and obey Pan's maximum principle. Therefore, it should be more rational than the traditional LEMs.

Conclusion

This study proposed a novel model that combines the critical unstable condition and stress analysis for the stability analysis of a given slip surface. The new model does not require the interslice assumption and can solve many problems that the traditional LEMs cannot solve. In addition to its superior accuracy, one of the highlights of the model is that the FOS of the slip surface can be obtained simultaneously with the displacement field by solving the nonlinear equations formed by the model directly. Although the FEM was employed as the discretization technique in this study, other

numerical approaches, for example, the boundary-element method, are also effective. Some specific conclusions of this study are as follows:

1. For planar slip surfaces, the FOS obtained by the proposed method was found to be very consistent with the analytical solution.
2. For planar and circular slip surfaces, although a large difference existed between the normal stress distributions on the slip surface obtained, respectively, from the proposed method and the MP, the FOSs calculated by these two methods were very close, which indicates that the FOSs of those two types of slip surfaces are insensitive to the normal stress distribution. For polyline slip surfaces, however, the FOSs obtained using the proposed method might be notably different from those by the MP methods. The reason is that the deformation of the slip body considered by the proposed method causes a significant change in the normal stress on the slip surface near the endpoints.
3. The variation of the FOS induced by excavation beneath the slip surface can be captured by the proposed methods. In contrast, the MP is insensitive to this process because its equilibrium equations are established on rigid slices.
4. The CUP concept introduced in this model has a clear physical meaning, and its behavior can be translated into a descriptive equation for the constraint of the relative tangential displacement of the slip surface in the critical state. In addition, its selection is in accordance with Pan's extremum principle.
5. Example 1 showed that the results, especially the normal stress distribution, from the proposed method and the SRM-slip were very consistent. The proposed method can quickly achieve convergence within two to three Newton iterations. In contrast, the SRM-slip requires more than 10 bisection iterations. Additionally, the FOS from the SRM-slip appears to be susceptible to the unstable criterion.

Overall, the proposed method has a rigid theoretical basis. It not only avoids the interslice assumption but also broadens the application scope of the limit-equilibrium theory. Because the FEM is incorporated, it is competent for evaluating a wide range of slopes. Therefore, the proposed method is expected to be an effective and practical tool for slope stability analysis.

Acknowledgments

References

Ahmed, A., Ugai, K., and Yang, Q. Q. (2012). "Assessment of 3D slope stability analysis methods based on 3D simplified Janbu and Hovland methods." *Int. J. Geomech.*, 10.1061/(ASCE)GM.1943-5622.0000117, 81–89.

Bai, B., Yuan, W., and Li, X.-C. (2014). "A new double reduction method for slope stability analysis." *J. Cent. South Univ.*, 21(3), 1158–1164.

Belytschko, T., and Black, T. (1999). "Elastic crack growth in finite elements with minimal remeshing." *Int. J. Numer. Methods Eng.*, 45(5), 601–620.

Bishop, A. W. (1955). "The use of the slip circle in the stability analysis of slopes." *Géotechnique*, 5(1), 7–17.

Brown, C. B., and King, I. P. (1966). "Automatic embankment analysis: Equilibrium and instability conditions." *Géotechnique*, 16(3), 209–219.

Burden, R. L., and Faires, J. D. (2011). *Numerical analysis*, 9th Ed., Brooks/Cole, Boston.

Chen, Z. (1998). "On Pan's principles of soil and rock stability analysis." *J. Tsinghua Univ. Sci. Technol.*, 38(3), 1–4.

Chen, Z. (2003). *Soil slope stability analyses—Theory, method and programs*, Water Power Press, Beijing.

Cheng, Y. M., Lansivaara, T., and Wei, W. B. (2007). "Two-dimensional slope stability analysis by limit equilibrium and strength reduction methods." *Comput. Geotech.*, 34(3), 137–150.

Cheng, Y. M., Zhao, Z. H., and Wang, J. A. (2008). "Realization of Pan Jiazheng's extremum principle with optimization methods." *Chin. J. Rock Mech. Eng.*, 27(4), 782–788.

Dawson, E. M., Roth, W. H., and Drescher, A. (1999). "Slope stability analysis by strength reduction." *Géotechnique*, 49(6), 835–840.

Donald, I. B., and Giam, P. (1992). "The ACADS slope stability programs review." *Proc., 6th Int. Symp. on Landslides*, D. H. Bell, ed., A. A. Balkema, Rotterdam, Netherlands, 1665–1770.

Fredlund, D. G., Scoular, R. E. G., and Zakerzadeh, N. (1999). "Using a finite element stress analysis to compute the factor of safety." *Proc., 52nd Canadian Geotechnical Conf.*, Canadian Geotechnical Society, Richmond, BC, Canada, 73–80.

Ge, X.-R. (2010). "The vector sum method: A new approach to calculating the safety factor of stability against sliding for slope engineering and dam foundation problems." *Advances in environmental geotechnics*, Springer, New York, 99–110.

Griffiths, D. V., and Lane, P. A. (1999). "Slope stability analysis by finite elements." *Géotechnique*, 49(3), 387–403.

Hirmand, M., Vahab, M., and Khoei, A. R. (2015). "An augmented Lagrangian contact formulation for frictional discontinuities with the extended finite element method." *Finite Elem. Anal. Des.*, 107, 28–43.

Isakov, A., and Moryachkov, Y. (2014). "Estimation of slope stability using two-parameter criterion of stability." *Int. J. Geomech.*, 10.1061/(ASCE)GM.1943-5622.0000326.

Janbu, N. (1975). "Slope stability computations." *Int. J. Rock Mech. Min. Sci. Geomech. Abstr.*, 12(4), 67.

Kulhawy, F. H. (1969). "Finite element analysis of the behavior of embankments." Ph.D. thesis, Univ. of California, Berkeley, CA.

Liu, S. Y., Shao, L. T., and Li, H. J. (2015). "Slope stability analysis using the limit equilibrium method and two finite element methods." *Comput. Geotech.*, 63, 291–298.

Liu, Y., Wang, C., and Yang, Q. (2012). "Stability analysis of soil slope based on deformation reinforcement theory." *Finite Elem. Anal. Des.*, 58, 10–19.

Matsui, T., and San, K.-C. (1992). "Finite element slope stability analysis by shear strength reduction technique." *Soils Found.*, 32(1), 59–70.

Morgenstern, N. R., and Price, V. E. (1965). "The analysis of the stability of general slip surfaces." *Géotechnique*, 15(1), 79–93.

Naylor, D. J. (1982). "Finite elements and slope stability." *Numerical methods in geomechanics*, J. B. Martins, ed., Springer, New York, 229–244.

Simo, J. C., and Laursen, T. A. (1992). "An augmented Lagrangian treatment of contact problems involving friction." *Comput. Struct.*, 42(1), 97–116.

SLIDE [Computer software]. Rocscience, Toronto.

Spencer, E. (1967). "A method of analysis of the stability of embankments assuming parallel inter-slice forces." *Géotechnique*, 17(1), 11–26.

Wang, W., Yuan, W., Li, X.-C., and Bai, B. (2016). "Evaluation approach of the slope stability based on deformation analysis." *Int. J. Geomech.*, 10.1061/(ASCE)GM.1943-5622.0000528.

Yuan, W., et al. (2016). "An approach to determining critical slip surface based on displacement field analysis." *Rock Soil Mech.*, 37(6), 1791–1798.

Zheng, H., Liu, D. F., and Li, C. G. (2005). "Slope stability analysis based on elasto-plastic finite element method." *Int. J. Numer. Meth. Eng.*, 64(14), 1871–1888.

Zheng, H., Sun, G., and Liu, D. (2009). "A practical procedure for searching critical slip surfaces of slopes based on the strength reduction technique." *Comput. Geotech.*, 36(1–2), 1–5.

Zienkiewicz, O. C., Humpheson, C., and Lewis, R. W. (1975). "Associated and non-associated visco-plasticity and plasticity in soil mechanics." *Géotechnique*, 25(4), 671–689.